



Severe plastic deformation of tubular AA 6061 via equal channel angular pressing

D.M. Jafarlou^{a,b}, E. Zalnezhad^{c,*}, M.A. Hassan^{a,b,d}, M.A. Ezazi^{a,b}, N.A. Mardi^{a,b}, A.M.S. Hamouda^e, M. Hamdi^{a,b}, G.H. Yoon^c

^a Department of Mechanical Engineering, Faculty of Engineering, University of Malaya, Kuala Lumpur 50603, Malaysia

^b Centre of Advanced Manufacturing & Material Processing (AMMP), Kuala Lumpur 50603, Malaysia

^c Department of Mechanical Convergence Engineering, Hanyang University, 222 Wangsimni-ro, Seongdong-gu, Seoul 133-791, Korea

^d Department of Mechanical Engineering, Faculty of Engineering, Assiut University, Assiut 71516, Egypt

^e Mechanical and Industrial Engineering Department, College of Engineering, Qatar University, P.O. Box 2713, Doha, Qatar

ARTICLE INFO

Article history:

Received 17 March 2015

Received in revised form 14 October 2015

Accepted 6 November 2015

Available online 7 November 2015

Keywords:

Severe plastic deformation

Equal channel angular pressing

Tubular AA 6061

Plastic instability

Grain refinement

Torsion test

ABSTRACT

Various severe plastic deformation (SPD) processes have been developed to produce metal tubes with ultrafine grain (UFG) structures. However, most techniques are complex and limited to working with components that are short in length to avoid tube failure during SPD processes. To overcome such limitations, this study suggests the use of an equal channel angular pressing (ECAP) process for the production of tubular aluminum alloy 6061. To mitigate plastic instability effects such as tube buckling and fracture during processing, hydraulic oil was used to fill the tube cavity. Finite element analysis (FEA) using Abaqus/Explicit 6.13 was carried out to examine the feasibility of the proposed method and deformation mechanism during ECAP. A series of investigations were performed, including: microstructure analysis, torsion, and micro hardness tests to evaluate the effects of tube-ECAP treatment. Test results indicated that the resultant 60% reduction in grain size led to significant mechanical property improvements including yield shear strength, ultimate shear strength, and microhardness. However, the ductility of the material decreased slightly for the ECAP-treated samples. To resolve this issue, a heat treatment process using the T6 method was performed, leading to a notable ductility enhancement in addition to further improvements in shear strength and microhardness.

© 2015 Elsevier Ltd. All rights reserved.

1. Introduction

During the last two decades, significant focus has been directed toward severe plastic deformation (SPD) as a direct method to produce bulk metals with ultrafine grain (UFG) structures. The principal SPD mechanism is to impose an ultra large plastic strain through the application of extremely high pressures at relatively low operating temperatures [1]. In this way, fractures originating from large shear plastic strain are avoided, since the shape of the bulk material remains unchanged after deformation and stress triaxiality does not exceed the effective plastic strain [2]. The ultra-large plastic strain introduced to the bulk metal during SPD is able to refine coarse grains (CG) and constitute ultrafine microstructures with grain sizes less than 100 nm [3].

The ultrafine grain metals yielded by SPD cannot be reproduced via conventional thermo-mechanical treatment (TMT) methods. As a result, SPD-processed metals exhibit a suitable combination of mechanical properties compared to metals with refined grain structures produced through conventional TMT processes [4].

Moreover, SPD processes are able to mitigate residual porosity and contamination defects in the final product which are frequently observed with powder based methods. Additionally, SPD techniques have great potential to be implemented in the mass production of UFG metallic materials [5].

Various SPD processes including equal channel angular pressing (ECAP), accumulative roll bonding (ARB), high pressure torsion (HPT), multi-axial forging and twist extrusion have been developed to fabricate UFG metals, which were reviewed in detail by Estrin and Vinogradov [6].

With this regard, a variety of SPD processes, such as tubular channel angular pressing (TCAP) [7], tube channel pressing (TCP) [8], high pressure tube twisting (HPTT) [9], tube cyclic extrusion compression (TCEC) [10], and stagger spinning [11] have been developed to produce UFG structures with tubular geometries. Tubular materials with UFG structures can be successfully produced via these methods; however, limitations such as low production rates, material inhomogeneity, short lengths of the final product, and SPD process complexity have restricted their widespread applicability for mass production.

Among the various SPD techniques for bulk material processing, ECAP has attracted particular attention due to its exceptional scaling

* Corresponding author.

E-mail address: erfan@hanyang.ac.kr (E. Zalnezhad).

potential for various industrial applications, including its ability to apply the highest plastic strain [12]. In a prior study, the ECAP process was modified to produce pure titanium components with UFG structures, in which sand-filled titanium tubes were extruded through a die with a 150° channel angle [13]. In another study, pure tubular copper with an initial wall thickness of 3.5 mm was successfully ECAP-treated with a flexible polyurethane rubber pad [14]. Microhardness results from this study revealed a 32% and 57% improvement after the first and fourth passes, respectively.

The objective of the research presented herein is to modify the ECAP process for the severe plastic deformation of tubular AA 6061 using a die with 120° channel and 22° corner angles. In order to prevent failures such as tube buckling, crumpling, and fracturing during processing, the workpiece cavity was filled with hydraulic oil (SAE 30). To examine the tube deformation mechanism during ECAP processing and to evaluate the possibility of tube fracture as a result of plastic instability, numerical simulations were carried out using an explicit elasto-plastic package, Abaqus 6.13. Experimental procedures were subsequently designed based on the results obtained via finite element analysis (FEA), and the influence of the proposed SPD process on the mechanical

properties and microstructure evolution of tubular AA 6061 was investigated. Furthermore, the influence of double treatment, including SPD and heat treatment (HT) using the T6 technique, on mechanical properties and microstructure evolution was considered.

2. The principle of tube-ECAP

A new method based on ECAP was developed for grain refinement of tubular metallic components. The principle of tube-ECAP, illustrated in Fig. 1(a), is based on the process of pressing a tubular workpiece through a die with a channel angle of φ and a corner angle of ψ . The outer surface of the tube is constrained by the channel surface of the die and the tube inner cavity is filled with hydraulic oil to prevent sample failure during processing.

In order to preserve and prevent hydraulic oil leakage within the cavity, the two inner tube ends were threaded, and a screw was fastened to one end of the tube with sealing tape. Finally, the workpiece cavity was completely filled with hydraulic oil and subsequently sealed by fastening with the second screw. Schematic representations of the initial workpiece are illustrated in Fig. 1(b).

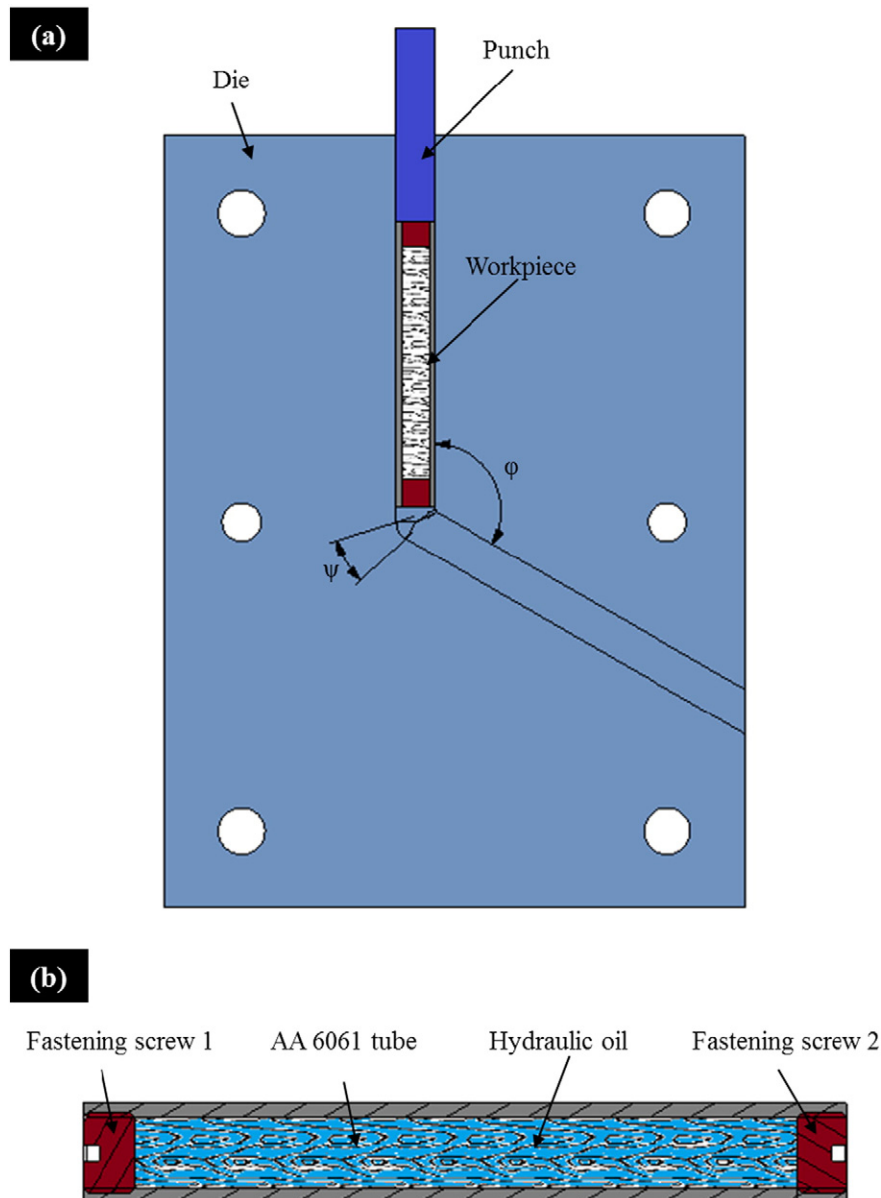


Fig. 1. Schematic illustration of (a) the tube-ECAP principle and (b) the assembly of the initial workpiece.

A severe shear was imposed to the tubular workpiece during extrusion through the point of intersection between two parts of the die channel. A large quantity of plastic strain accumulated in the workpiece as a result of the ultra-large shear stress. The deformation mode in this process was a simple shear, controlled by the die corner (ψ) and channel (φ) angles. According to the principle of processing and incompressibility of the applied hydraulic oil, the process precisely resembled conventional ECAP.

3. Experimental procedures

3.1. Base materials

The 6061-O aluminum alloy (wt.%: 95.85 Al, 1.2 Mg, 0.75 Si, 0.6 Fe, 0.4 Cu, 0.15 Mn, other elements <balance>) was used as the test material in this study. Due to the exceptional mechanical and metallurgical properties of this grade of aluminum alloy, including good weldability, proper affinity to various coatings, workability, and high corrosion resistance, AA6061-O has been extensively utilized in various industrial applications such as: construction (couplers, connectors, appliance fittings, and hinge pins), transportation (aircraft, marine, automotive fittings, brake pistons, hydraulic pistons), and electronics industries (electrical fittings and connectors). Furthermore, heat treatment hardening methods such as T6, T7, and T8 are also available for this grade of aluminum alloy [15–17].

Component mechanical properties, including yield strength (σ_y), ultimate tensile strength (σ_u), Young modulus (E), strain at peak stress (ϵ_u), Poisson's ratio (ν), work hardening exponent (n), and strength coefficient (k) were determined by conducting a number of tensile tests in accordance with ASTM standard E8/E8M-11 [18]. The measured elastic-plastic properties of AA6061-O are listed in Table 1.

In this study, the influence of ECAP and double treatment, including ECAP and T6 heat treatment, on the microstructure evolution and mechanical properties of ECAP-treated tubular AA6061-O were investigated. Three sample types (Table 2) were prepared for the experimental investigation.

3.2. Tube-ECAP processing and heat treatment

In this study, the die set with a 10 mm internal channel diameter was machined (final surface roughness of 0.8 μm) with a 120° channel angle and a 22° corner angle from bulk H13 tool steel, which was heat treated to achieve a hardness value of 610 H_v.

Segmented AA 6061-O tubes (75 mm length) filled with SAE 30 hydraulic oil were fed through a die channel into the die's abrupt angle using a punch coupled to a 100 kN press at 1 mm s⁻¹ at room temperature. The influence of internal heating during ECAP was investigated by other researchers [19]. Prior findings have shown that for pressing speeds of 0.18 mm s⁻¹, 1.8 mm s⁻¹, and 18 mm s⁻¹, the aluminum alloy experienced temperature growths of 1 °C, 45 °C, and 75 °C, respectively. Herein, the tube-ECAP process was carried out at room temperature under a constant pressing speed of 1 mm s⁻¹, considerably minimizing heat generation during deformation. Furthermore, the die channel and aluminum alloy tube surfaces were lubricated with molybdenum disulfide (MoS₂) to minimize contact surface friction effects. Fig. 2 reveals the fabricated tool set and ECAP treated workpiece.

Moreover, in order to determine the effects of heat treatment, ECAP-treated workpieces were heat treated through the T6 procedure. For the T6 process, samples were solution treated at 520 °C for 1 h and

Table 2

Details with regard to the workpiece types used in the current study along with their corresponding nomenclature.

Sample	Process nomenclature
1	As-received (raw material)
2	ECAP
3	ECAP + HT

instantaneously quenched with water. The workpieces were artificially aged at 170 °C for 8 h.

3.3. Sample preparation for mechanical and metallurgical analysis

In order to prepare the samples for metallographic etching, standard grinding procedures (up to 2500 grit) followed by mirror polishing with an alumina suspension (down to 0.1 μm) were carried out on sample cross sections. After the final polishing step, samples were rinsed with distilled water, cleaned with a soapy water soaked cloth, rinsed again, and sonicated in ethanol for 5 min.

The etching process was comprised of two successive steps. Initially, the samples were pre-etched for 1 min with a solution made from the following: 1 g NaOH, 1 g NaF, and 100 ml distilled water. Afterwards, the samples were rinsed with distilled water, ethanol, and immersed in Keller's reagent (1 ml HF, 1.5 ml HCl, 2.5 ml HNO₃, and 95 ml distilled water) for 2 min at 25 °C. Finally, the etched samples were rinsed again with water and cleaned with ethanol to be prepared for microstructural investigation via optical microscopy.

After etching, quantitative image analysis (ImageJ 1.47v software, Wayne Rasband National Institute of Health, USA) was employed to measure the average grain size for various samples. Using image analysis software, all images were calibrated by converting the length of the image scale bar from pixels to microns. In order to measure the average grain size, a mean value of 60 grains was measured per sample and the statistical deviation from the mean grain diameter was reported as the standard error.

Following ECAP, all workpieces (Table 2) were prepared for torsion testing according to the ASTM standard E143-13 [20] in order to study their torsional strength (yield and ultimate value). Although torsion testing has not been extensively utilized for the evaluation of mechanical properties as much as tensile testing [21], this destructive test can

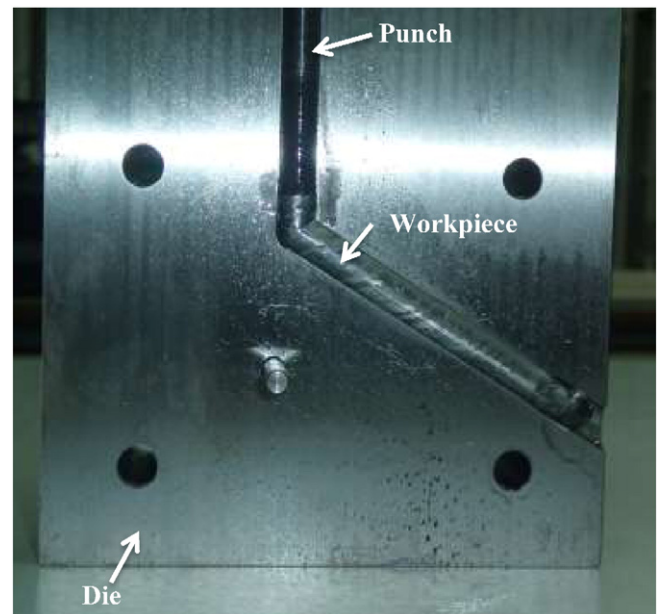


Fig. 2. Tube illustration after ECAP and the fabricated tool set, including die and punch.

Table 1
Elastic-plastic properties of AA6061-O.

Mechanical properties	σ_y (MPa)	σ_u (MPa)	E (GPa)	ϵ_u	ν	n	k (MPa)
Measured value	55	125	70	0.27	0.33	0.2	105

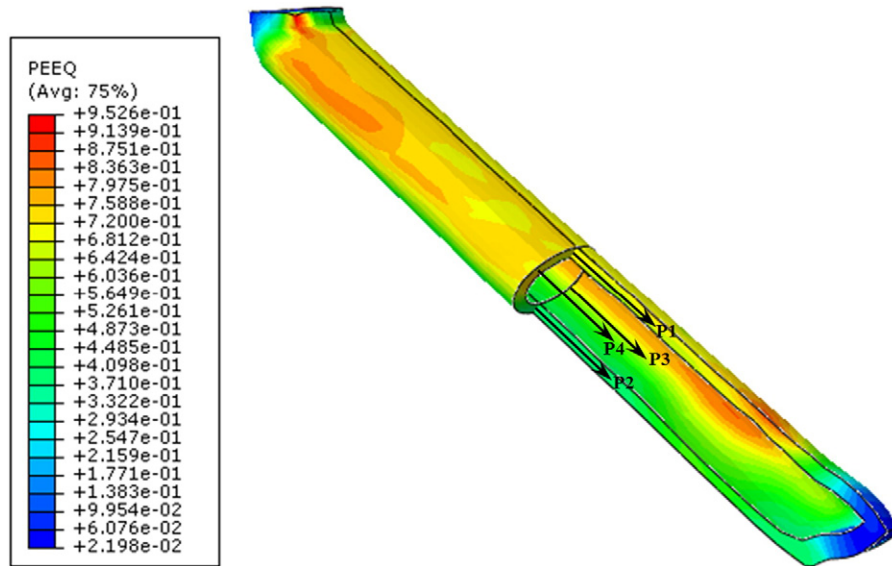


Fig. 3. Distribution of the equivalent plastic strain (EPS).

evaluate the mechanical properties of tubular components processed through SPD by allowing for an examination of the full-size components, unlike other methods such as the ring hoop tensile test [22] or ring test [23].

For the purpose of visual characterization, a Phenom ProX scanning electron microscope was utilized to observe the microscopic features of failed samples following torsional testing.

Vickers microhardness tests with an applied load and duration of 1 kgf and 10 s, respectively, were performed according to the ASTM E384-11e1 [24] on various tube cross sections via “Mitutoyo AVK-C200” equipment. The mean hardness for each sample was obtained from 4 different indentation lines across the tube cross sections. Additionally, to examine the variation trend of hardness across the thickness of the tube cross sections, Vickers indentations were performed at 6 equidistant points along the radius. During hardness tests, to avoid interference with work-hardened regions of previous indentations, an offset of 2.5 times the indentation diagonal was accounted for between two successive hardness tests. Based on the length of the indentation diagonal measured under the optical microscope in addition to the applied load, the following equation was employed to evaluate the Vickers hardness (H_v):

$$H_v = \frac{(1.8544F)}{d^2} \quad (1)$$

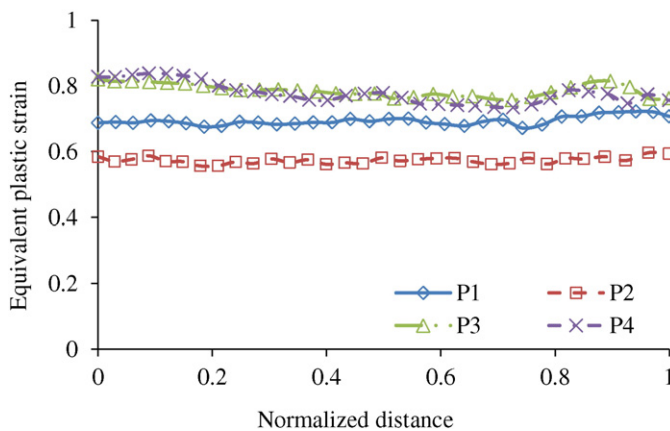


Fig. 4. Distribution of the effective plastic strain (EPS) in the longitudinal direction along paths P1–P4.

where F represents the test load (kgf) and d is the average length of two indentation diagonals (mm).

4. Finite element modeling

The elasto-plastic finite element package, Abaqus 6.13, was used in this study to simulate a newly proposed SPD method for tubular AA 6061-O components using ECAP. In order to precisely determine the workpiece deformation pattern during processing and to facilitate a comparison between numerical and experimental results, a 3D FEA model was prepared in accordance with the material properties and geometrical dimensions of the experimental workpieces.

The mechanical properties used in the simulation were obtained from the tensile testing data presented in Table 2. Additionally, the hardening behavior of AA 6061-O was expressed as $\bar{\sigma} = 105\bar{\epsilon}^{0.2}$, which was experimentally obtained by performing a number of tensile tests in accordance with ASTM standard E8/E8M-11 [18].

The FEA mesh configuration for the workpiece (tube) consisted of 4500 eight-node brick elements with reduced integration and

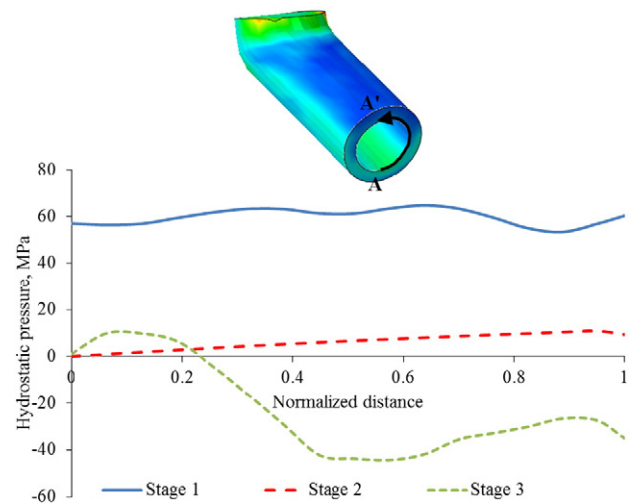


Fig. 5. Variation in hydrostatic pressure along path A–A' at stage one (punch stroke of 3.5 mm), stage two (punch stroke of 35 mm), and stage three (punch stroke of 70 mm).

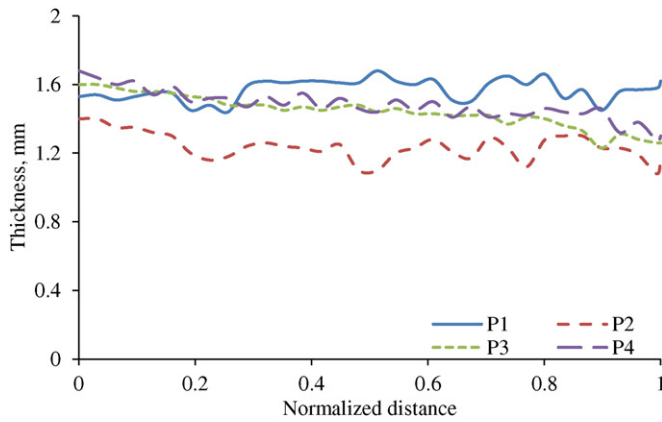


Fig. 6. Thickness distributions along the longitudinal direction for paths P1–P4.

hourglassing control (C3D8R). This element type allowed the workpiece to demonstrate reasonable results under severe deformation. Furthermore, Arbitrary Lagrangian–Eulerian (ALE) adaptive re-meshing with one sweep per increment was utilized throughout the simulation to maintain a high-quality mesh under deformation by allowing the mesh to move independently with respect to the underlying material.

Computational efficiency of the simulation under explicit procedures was enhanced by artificially increasing the density of the material via mass scaling. In order to avoid result errors due to amplified inertia forces, the ratio of kinetic energy to internal energy was monitored during the simulation. This fraction was negligible for the current simulation and confirmed the quasi-static response of the explicit method with applied step time and mass scaling.

Contact between the tool set and workpiece was defined using the penalty algorithm by considering the rigid parts (die and punch) and deformable parts as the master and slave surfaces, respectively. The Coulomb constant μ in the contact interfaces was set to 0.1, which was in the range of a typical ECAP process [25].

The response of the tube under SPD depended on the shear imposed by the die channel's abrupt angle in addition to the pressure exerted by the fluid, which in turn was affected by tube deformation. Therefore, mechanical response predictions for the hydraulic oil-filled cavity were important for the simulation. With this regard, the Abaqus 6.13 "Surface-based fluid cavity" module was utilized to model the hydraulic oil-filled workpiece cavity. The compressibility of the hydraulic oil was

Table 3

The corresponding dimensions (in mm) of the sections shown in Fig. 7.

	t_1	t_2	t_3	t_4	D_1	D_2
A-A'	1.46	1.43	1.55	1.35	10.03	10.09
B-B'	1.49	1.49	1.54	1.44	10.16	10.05
C-C'	1.59	1.57	1.65	1.30	10.15	10.02

introduced by defining the bulk modulus. The density of the "SAE 30" hydraulic oil and the bulk modulus were considered to be 850 kg/m³ and 1.5 GPa, respectively, at 20 °C [26].

5. Results and discussion

5.1. Finite element analysis

5.1.1. Evolution of equivalent plastic strain

In order to ensure grain refinement during ECAP, the strain value accumulated in the sample could be estimated by accounting for the corner (ψ) and channel (φ) angles. The distortion of an arbitrary element in x - y plane can be describe by engineering shear strain (γ_{xy}) according to Iwahashi et al. [27]:

$$\gamma_{xy} = 2 \cot(\varphi/2 + \psi/2) + \psi \operatorname{cosec}(\varphi/2 + \psi/2). \quad (2)$$

The equivalent plastic strain $\bar{\epsilon}$ in general form is represented by:

$$\bar{\epsilon} = \sqrt{2/3} \left[\epsilon_x^2 + \epsilon_y^2 + \epsilon_z^2 + \frac{\gamma_{xy}^2 + \gamma_{yz}^2 + \gamma_{zx}^2}{2} \right]^{1/2}. \quad (3)$$

By substituting Eq. (2) in Eq. (3) and considering $\epsilon_x = \epsilon_y = \epsilon_z = \gamma_{yz} = \gamma_{zx} = 0$ the equivalent strain, $\bar{\epsilon}$ after one pass is given by [27]:

$$\bar{\epsilon} = \frac{1}{\sqrt{3}} (2 \cot(\varphi/2 + \psi/2) + \psi \operatorname{cosec}(\varphi/2 + \psi/2)). \quad (4)$$

Since the same amount of strain is accumulated in the sample after each pass, equivalent plastic strain, $\bar{\epsilon}$ after P pass is calculated as [12]:

$$\epsilon_{equ} = \frac{P}{\sqrt{3}} (2 \cot(\varphi/2 + \psi/2) + \psi \operatorname{cosec}(\varphi/2 + \psi/2)). \quad (5)$$

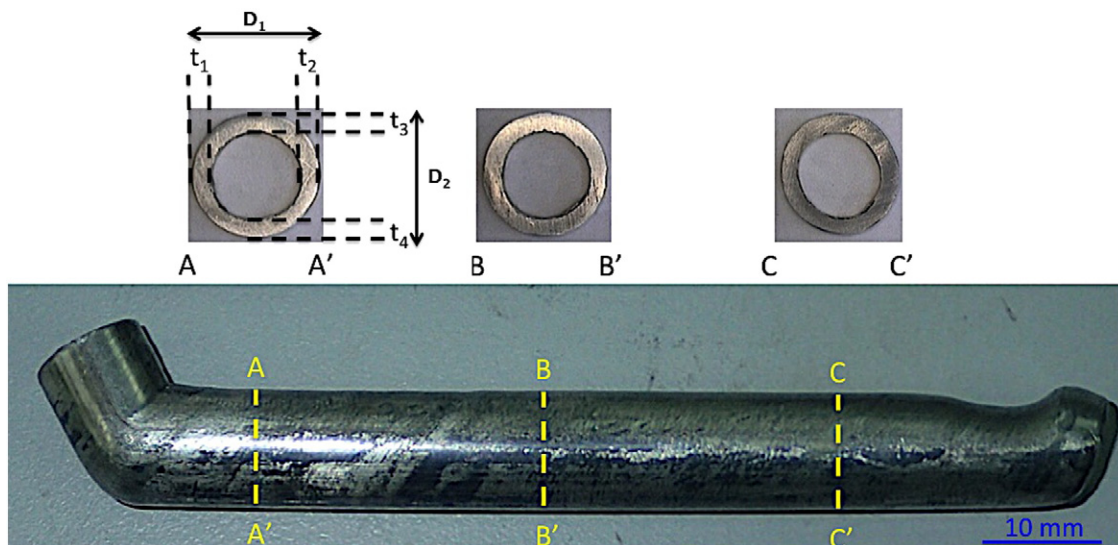


Fig. 7. An overall view of the ECAP-treated tubular workpiece in addition to cross-sectional views of the three different sections.

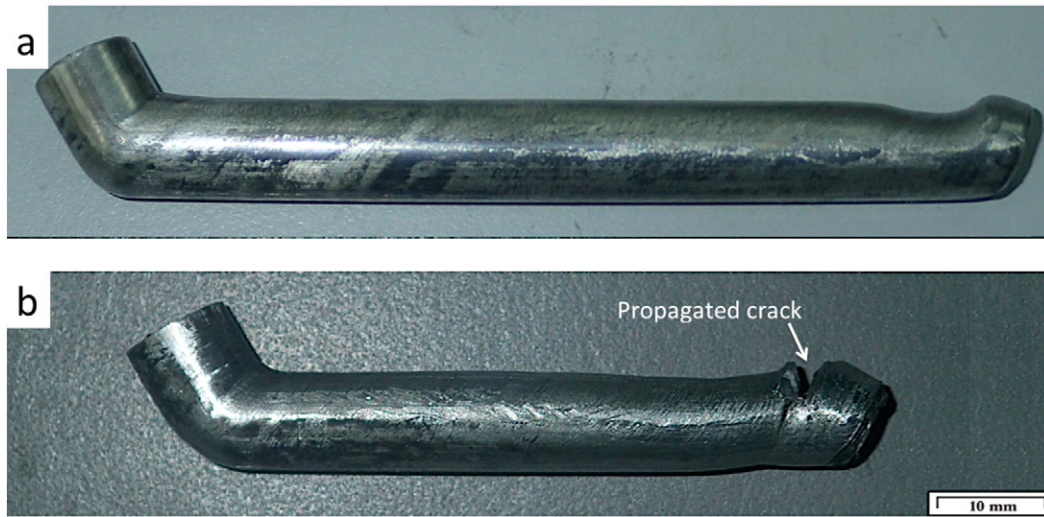


Fig. 8. (a) Successful and (b) failed ECAP-treated tubes.

For the die used in this study with $\psi = 22^\circ$ and $\varphi = 120^\circ$, and considering one pass of ECAP, Eq. (5) estimated the equivalent plastic strain (EPS) to be 0.63. This value was a reasonably large strain that could effectively refine the grains of tubular components via more straightforward processes compared with other common techniques such as TCAP [7], TCP [8], HPTT [9], TCEC [10], and ASB [28].

As the effects of friction and strain inhomogeneity were not considered in Eq. (2), the distribution of EPS was calculated numerically through FEA. Fig. 3 illustrates the distribution of EPS throughout the tube after completing the ECAP process, clearly showing that the proposed method is capable of exerting an acceptably high amount of EPS to the workpiece. The accumulated EPS was approximately 0.7 at the upper surface section of the tube, which was in contact with the corner angle, whereas this value reduced down to nearly 0.57 at the lower surface of the tube (the region that was in contact with the channel angle). Accordingly, the value of EPS calculated based on the analytical equation (Eq. (2)) revealed an approximate value of 0.63, which could roughly be considered as the average FEA outcome value mentioned above.

In order to quantify the homogeneity of EPS in the tube after ECAP, EPS was analyzed at the middle of the tube thickness along four different longitudinal paths (directions: P1, P2, P3, and P4) as depicted in Fig. 3, with the results illustrated in Fig. 4. From this figure, the homogeneity of EPS was evident for each path. However, specifically considering each direction, moderate inhomogeneity in EPS was apparent

along direction P2, exhibiting a relatively low value of ~0.57, while directions P3 and P4 exhibited higher values of ~0.8.

Microstructure homogeneity and hardness uniformity were proportional to the homogeneity of EPS, which was imposed within the workpiece via ECAP [29]. The strain inhomogeneity index (C_i) was proposed by Li et al. [30] as a factor to quantify the degree of deformation inhomogeneity as follows:

$$C_i = \frac{\bar{\epsilon}_{\max}^p - \bar{\epsilon}_{\min}^p}{\bar{\epsilon}_{\text{ave}}^p} \quad (6)$$

where $\bar{\epsilon}_{\max}^p$, $\bar{\epsilon}_{\min}^p$, and $\bar{\epsilon}_{\text{ave}}^p$ indicate the maximum, minimum, and average EPS, respectively. The C_i values in the longitudinal direction of the tube for all four paths (P1, P2, P3, and P4) were approximately 5%. However, the value of C_i for the entire tube was almost 30%, indicating higher homogeneity compared to other methods including HPTT [9].

5.1.2. Hydrostatic stress and thickness distribution analysis

FEA results in Fig. 5 revealed that the hydrostatic pressure over the internal surface of the tube varied during pressing. With this regard, the hydrostatic pressure distribution at the inner surface of the tube along path A-A' at a punch stroke of 3.5 mm (stage one), 35 mm (stage two), and 70 mm (stage three) was measured and summarized

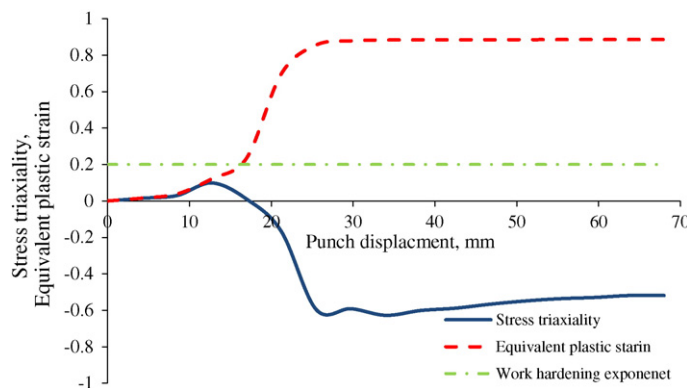


Fig. 9. Calculated equivalent plastic strain (EPS) and stress triaxiality versus punch displacement at the point of crack initiation as predicted from FEA-simulation.

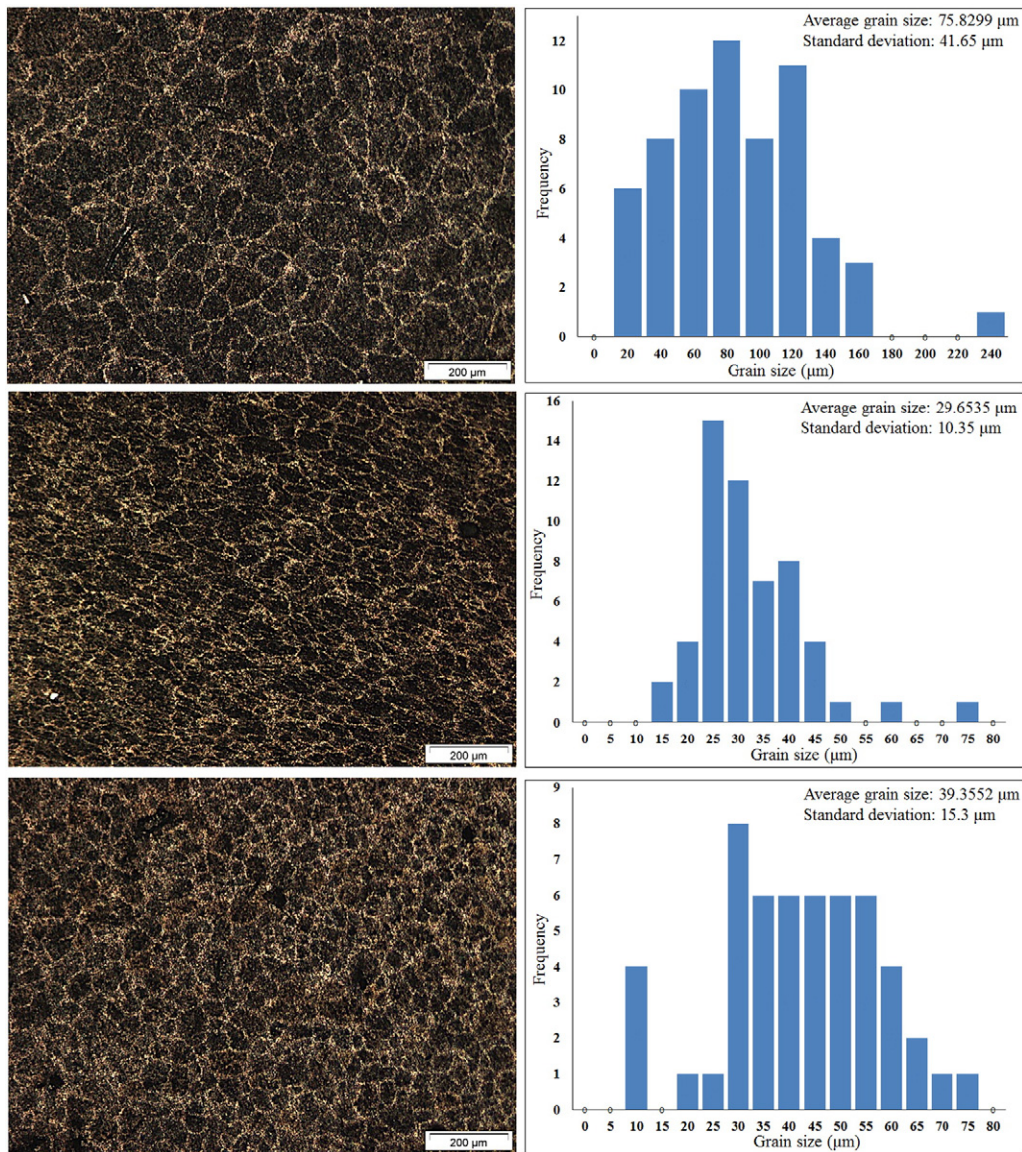


Fig. 10. Optical micrographs and grain size distributions obtained from quantitative image analysis for (a, b) sample 1 (as received), (c, d) sample 2 (ECAP-treated), and (e, f) sample 3 (double-treated).

in Fig. 5. The hydrostatic pressure imposed on the workpiece at the onset of dead zone formation when the punch stroke was 3.5 mm (stage one) consistently reached a value of ~60 MPa, signifying that the hydraulic oil was under pressure.

At a punch stroke of 35 mm (stage two), the hydrostatic pressure decreased significantly and reached zero at the bottom internal surface of the tube (point A). However the hydrostatic pressure increased slightly across the internal surface along the path A–A', reaching a value of ~10 MPa at the upper internal surface of the tube (point A'). Finally, it was observed with a punch stroke of 70 mm (stage three), that the hydrostatic pressure was positive at the lower internal tube surface adjacent to the die corner angle (point A). However, by moving toward point A', the hydrostatic pressure exhibited negative values at the internal tube surface. This variation in hydrostatic pressure indicated that the oil pressure varied during ECAP and affected the tube geometry.

In order to further investigate the effect of oil pressure on geometry, variations in the tube wall thickness were measured. Fig. 6 demonstrates the thickness distributions along the P1, P2, P3, and P4 directions (Fig. 3). The thickest section was observed around the upper part of the tube along the P1 direction. However, by moving toward the bottom

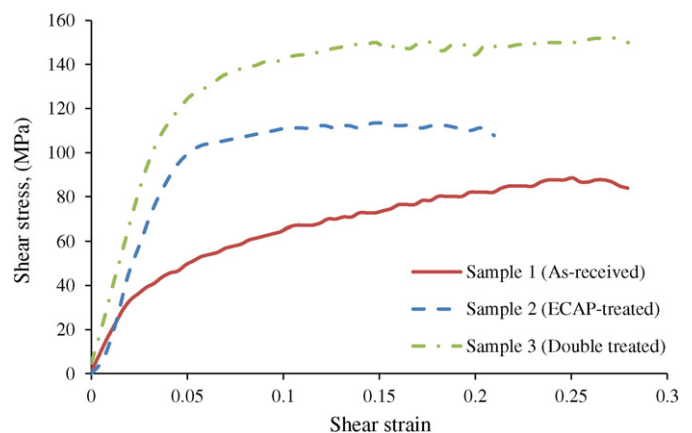


Fig. 11. Shear stress–strain curves at room temperature for the as-received, ECAP-treated, and double-treated (ECAP + heat treated) workpieces after one ECAP cycle.

section of the tube, the thickness decreased along the P2 direction. This result could be attributed to a non-uniform distribution of hydrostatic pressure along the inner surface of the tube (Fig. 5). To explain in detail, the upper section of the tube along path P1 experienced a negative hydrostatic pressure during ECAP (Fig. 5), leading to an accumulation of material within this region. On the contrary, the bottom section of the tube continuously experienced a positive hydrostatic pressure as the punch reached higher strokes, leading to tube thinning along the P2 direction. Numerical measurements indicated a variation in uniform thickness along the P3 and P4 directions with a 1.5 mm minimum wall thickness difference between the as-received and ECAP treated tubes for both cases.

Fig. 7 presents the overall view of the ECAP-treated tubular workpiece in addition to cross-sectional views for three different sections. Variations in wall thickness and diameter of the ECAP-treated tubes were measured and summarized in Table 3. As the results showed, the tube diameters (D_1 and D_2) remained constant without exhibiting ovality after ECAP. Furthermore, thickness measurements in the horizontal direction (t_1 and t_2) signified an insignificant reduction in tube wall thickness. However, a thickening of the tube wall thickness was observed in the upper section of the tube (t_3), reaching up to 0.15 mm in section C–C'. The lower sectional tube measurements were indicative of a thinning phenomenon resulting from an excessive plastic upflow of material, exhibiting a ~ 0.2 mm reduction in wall thickness (t_4). These variations in tube thickness which were in accordance with the FEA outputs (Fig. 6) explained the observation of a slight degree of tube ovality and eccentricity.

5.2. Plastic instability

The onset of plastic instability ($d\sigma/d\varepsilon = \sigma$) in tubular AA6061 was studied in order to characterize the probability of tube fracture during the ECAP process. Machining errors due to precision limitations, excessive friction between the tube and channel die, structural inhomogeneity of materials, and unfit sealing of the tube and screw may result in the leakage of hydraulic oil, which could lead to the initiation of cracks, crack propagation, and eventually failure. Fig. 8 shows some examples of successful and failed tubular workpieces.

It is well known that ductile fracture is related to the ability of a metal to withstand a notable degree of deformation prior to fracture when the value of EPS exceeds the fracture strain value ($\bar{\varepsilon}_f$). Prior studies have shown that fracture strain could be correlated to the work hardening exponent (n), obtained via uniaxial testing according to the Considère criterion [31], or in case of complex stress states such as ECAP, through stress triaxiality [32].

To explain in detail, for a Hollomon material, the power law equation can be used to find the end of uniform elongation as:

$$\bar{\sigma} = K\bar{\varepsilon}^n \quad (7)$$

where K and n are the strength coefficient and work hardening exponent constants, respectively. The value of equivalent stress $\bar{\sigma}$ was calculated as:

$$\bar{\sigma} = \sqrt{1/2[(\sigma_1 - \sigma_2)^2 + (\sigma_2 - \sigma_3)^2 + (\sigma_3 - \sigma_1)^2]} \quad (8)$$

where σ_1 , σ_2 , and σ_3 were principle stresses values and the equivalent plastic strain ($\bar{\varepsilon}$) was obtained using Eq. (5).

Accordingly for the case of uniaxial tension, at the end of uniform elongation, the slope of the stress/strain curve was zero. Therefore, we could use Eq. (7) to obtain the load (P) as:

$$\ln P = \ln k + n \ln \bar{\varepsilon} + \ln A_0 - \bar{\varepsilon} \quad (9)$$

where A_0 was the initial area of the tensile test cross section. We can now set Eq. (9) equal to zero in order to obtain the uniaxial tension

test criterion:

$$\frac{d(\ln P)}{d\bar{\varepsilon}} = \frac{n}{\bar{\varepsilon}} - 1 = 0. \quad (10)$$

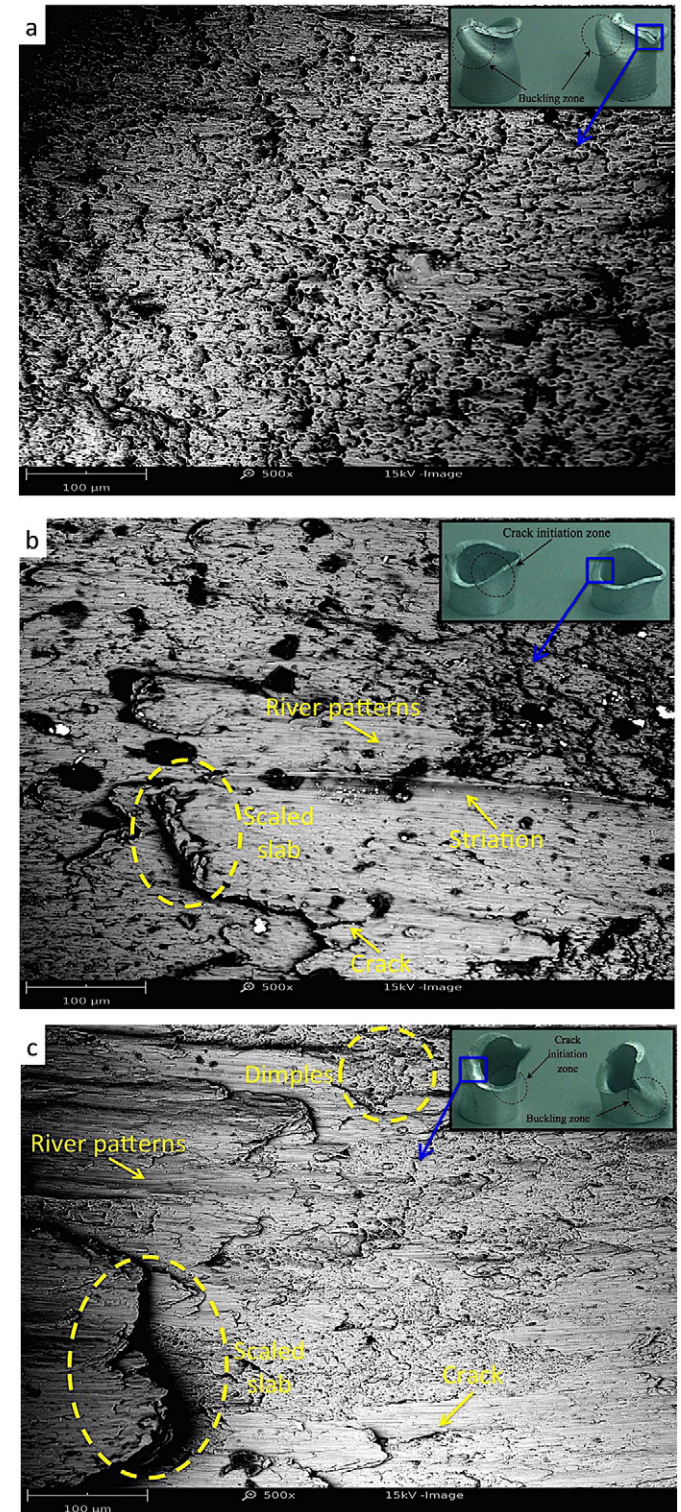
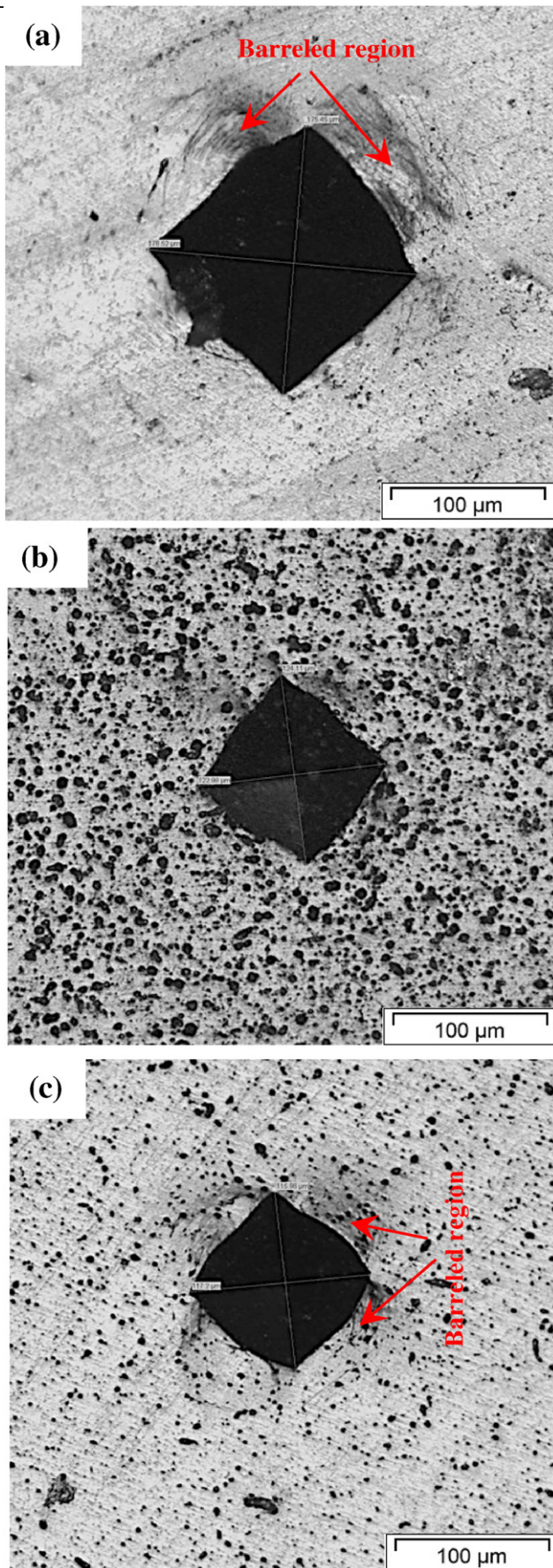


Fig. 12. Overview and magnified micrographs of failed samples for the (a) as-received, (b) ECAP-treated, and (c) double-treated (ECAP + heat treated) workpieces.



Therefore, according to the uniaxial tension criterion, ductile fracture at the fracture strain value ($\bar{\epsilon}_f$) could be predicted when:

$$n = \bar{\epsilon} = \bar{\epsilon}_f. \quad (11)$$

As evident, Eq. (11) was independent of stress triaxiality, which significantly affected the occurrence of ductile fracture in the case of three-dimensional processes such as tube ECAP. Stress triaxiality (η) was represented as follows:

$$\eta = \frac{\sigma_m}{\bar{\sigma}}, \quad (12)$$

where $\sigma_m = (\sigma_1 + \sigma_2 + \sigma_3)/3$ is the hydrostatic stress. Hancock and Mackenzie [33] found that the potential for ductile fracture decreased by increasing the stress triaxiality. Therefore, the fracture strain ($\bar{\epsilon}_f$) and stress triaxiality (η) were inversely proportional:

$$\bar{\epsilon}_f \propto \exp\left(-\alpha \frac{\sigma_m}{\bar{\sigma}}\right), \quad (13)$$

where α is the material constant. In order to evaluate the potential for fracture in this study, the point under the greatest amount of strain was monitored during FEA. EPS and stress triaxiality (η) values were plotted with respect to punch displacement, as illustrated in Fig. 9. Accordingly, tube failure occurred if the stress triaxiality value exceeded the fracture strain ($\bar{\epsilon}_f$) during the punch stroke.

As evident from Fig. 9, tube stress triaxiality (η) increased during the onset of the process due to static friction conditions and the formation of a dead zone reaching a maximum value of almost 0.11 at a punch displacement of 12 mm, with a relative EPS of ~0.12. However, the value of EPS was considerably less than expected based on the uniaxial tension fracture criterion ($n = 0.2 > \bar{\epsilon}$). At a punch displacement of 18 mm, the stress triaxiality value decreased down to zero, and became negative as the process continued, providing a safe condition during the ECAP process.

5.3. Microstructure analysis

The microstructure and grain size distribution of various samples are illustrated in Fig. 10. The microstructure of the as-received AA 6061-O (sample 1) with deformation free grains as a result of annealing and an average grain size of 75.8 μm can be seen in Fig. 10(a). The coarse grains were homogeneously distributed in the extrusion direction (ED) and normal direction (ND) with relatively equiaxed structures. Moreover, from an analysis of grain size in Fig. 10(b), the existence of a few grains with a diameter of 240 μm and some finer grains (20 μm in diameter) were apparent. However, the majority of the grains appeared to be in the size range of 40 μm to 120 μm .

Fig. 10(c) shows the microstructure evolution of the tubular workpiece after a single ECAP pass. As seen in Fig. 10, the sample microstructure was remarkably different from the as-received workpiece due to the appearance of fine grains resembling a lamellar (or irregularly bent lamellar) morphology which were elongated in the shear direction, indicating that the imposed plastic strain led to a significant grain refinement in the AA 6061 structure after one cycle. Image processing results obtained from the ECAP-treated sample (Fig. 10(d)) revealed a mean grain diameter of 29.65 μm with the majority of grains being in the size range of 20 μm to 45 μm , showing a significant grain size reduction of 60% compared to the as-received workpiece.

Furthermore, the microstructure of the workpiece following double-treatment (ECAP + heat treatment) can be seen in Fig. 10(e). As a result of the heat treatment (T6) following ECAP, an overall increase in the mean grain diameter was observed and accompanied by a

Fig. 13. Optical images of indentations left on (a) as-received, (b) ECAP-treated, and (c) double-treated (ECAP and heat-treated) workpieces.

morphological conversion from elongated to equiaxed shapes, which could be attributed to in situ recovery processes [34]. Moreover, the T6 heat treatment process resulted in the formation of homogeneous microstructures in the double-treated workpiece with an average grain size of 39.35 μm (Fig. 10(f)). The T6 heat treatment was a three stage process and included the dissolution of soluble phases via annealing at 520 °C for 1 h, the development of supersaturated microstructures via quenching immediately after annealing, and the precipitation of solute atoms as a result of artificial age hardening (heating for 7 h at 170 °C). The first stage of the T6 process provided a possibility for the formation of mixed grains with various sizes (small sized grains in particular) and yielding recrystallized microstructures with newly formed grain boundaries. As a result of quenching (stage 2 in the T6 process), small-sized nucleated grains were surrounded by coarse grains which could contribute to the formation of bimodal microstructures. Due to this particular microstructure, the final material was able to simultaneously exhibit specific mechanical properties such as high ductility and strength [35,36].

5.4. Mechanical properties

5.4.1. Torsion test

Shear stress–strain curves resulting from the torsion test can be seen in Fig. 11. In the ECAP process, grains were refined due to extreme EPS imposed on the tube. Newly-formed fine grains with small sizes increased the grain boundary density, which could serve as an impeding factor to effectively resist the propagation of dislocations, causing a remarkable improvement in the strength of the workpiece considering the Hall–Petch equation [37]. As seen in Fig. 11, the yield shear strength and ultimate shear strength of the ECAP-treated workpiece improved considerably by factors of ~ 2.5 and ~ 1.4 , respectively, in comparison with the as-received workpiece. In the case of the double-treated workpiece, further progress was observed with regard to the yield shear strength and ultimate shear strength by factors of ~ 1.1 and ~ 1.3 compared to the ECAP-treated workpiece, respectively. On the other hand, research findings related to ductility after the SPD process were rather contradictory. Some researchers observed an enhanced ductility after SPD due to a combination of UFG effects and the formation of high-angle grain boundaries [38]. However, another study showed that the SPD process reduced ductility due to a strong localization of strain [39]. The torsion test results in the current study indicated that the ECAP process imparted a detrimental effect on ductility (ultimate twist at rupture) compared to the as-received workpiece. The results also showed that heat treatment after ECAP eliminated the negative effect of ECAP processing on ductility. A notable improvement in the ductility of ECAP-treated AA6061-O could be obtained by performing a post heat treatment process.

Visual examination of the failed samples at low and high magnifications was performed to assess the material ductility and morphology of the fractured surfaces. According to the results, the fractured sections could be classified into three categories: cross sections with ductile fractures, cross sections with brittle fractures, and fractured regions characterized by thin tube-wall buckling. To explain in detail, ductile fractures occurred due to a maximum exertion of shear stress (τ_{\max}) at a plane perpendicular to the longitudinal axis (tube axis), whereas brittle fractures occurred due to a maximum exertion of tensile stress ($\sigma_1 = \tau_{\max}$) at a plane with a 45° offset from the longitudinal axis, typically resulting in fractured sections with helicoid morphologies. The third failure mode observed after torsional testing was buckling, which occurred in the thin walls of tubular components due to membrane shear stress [40].

The failed workpieces after torsional testing can be seen in Fig. 12. Failure in the as-received workpiece occurred due to premature buckling prior to crack formation. It was deduced that premature buckling occurred due to the simultaneous effect of high ductility and low yield strength. At high magnification, rough surfaces with an array of

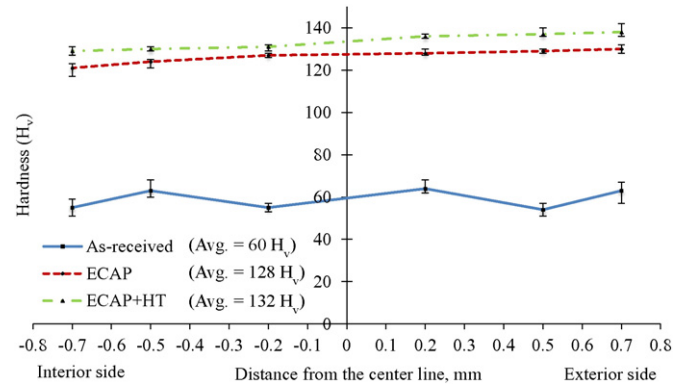


Fig. 14. Micro hardness values along the tube wall thickness for the as-received, ECAP-treated, and double-treated (ECAP + HT) samples.

successive dimples and voids were visible, characteristic of ductile fractures (Fig. 12(a)). Similar failure modes have been reported in prior research studies in the case of tubular components made from aluminum and steel [41]. However, the failed section of the ECAP-treated tube (Fig. 12(b)) provided evidence for a reduction in material ductility compared to the as-received workpiece with a 45° inclined fracture plane. SEM micrographs confirmed the same morphology at the micro scale by revealing features such as scaled slabs, river patterns, striations, and cracks. The failed sections of the double-treated workpiece (Fig. 12(c)) represented a mixed failure mode by showing traces of both ductile and brittle fracture. In this workpiece, the onset of crack nucleation occurred within highly distorted zones as a result of strain localization imposed by tube buckling. Correspondingly, under high magnification, the simultaneous emergence of ductile and brittle fractures became apparent.

5.4.2. Hardness

Figs. 13(a–c) reveal the micro hardness indentation examples for the as-received, ECAP-treated, and double-treated sample workpieces, respectively. It was evident that the size of the indentation left on the as-received workpiece was significantly larger than the indentation left on the ECAP-treated and double-treated workpieces. However, a comparison between Fig. 13(b) and Fig. 13(c) revealed a slight decrease in the indentation size as a result of heat treating after the ECAP process.

Hardness as a function of material strength and ductility was associated with grain size according to the Hall–Petch equation [37]. Based on the results reported in the literature [42], distortion of the indentation outline, characterized by material pile-up around the indentation, could be used as a basis for comparison between the average grain size of a workpiece.

Fig. 13(a) shows the Vickers indentation outline for the as-received sample. In this case, considerable material pile-up and ridging formed around the indentation boundary. Barreling effects as a result of these phenomena were observed for this workpiece, which could be associated with the coarse grain structure of the as-received material.

It could be clearly seen from Fig. 13(b) that the barreling effect disappeared from the ECAP-treated workpiece due to grain refinement. This phenomenon confirmed the decrease in material ductility following ECAP processing as well.

In the case of the double-treated workpiece, due to the T6 heat treatment process (recrystallization and evolution of equiaxed structures) resulting in a slight ductile recovery of the ECAP-treated workpiece, traces of the barreling effect could be observed around the indentations as seen in Fig. 13(c).

Due to moderate microstructural inhomogeneities represented by the standard deviation of the grain size analysis (Fig. 10), slight variations in hardness values were observed at different points of the various

samples according to their radial position. From Fig. 14, inconsistent variations in hardness values without a specific trend were evident in the case of the as-received workpiece, which was in accordance with the extended range of the grain size analysis standard deviation reported in Fig. 10(b). Although the hardness values exhibited a slight increasing trend toward the exterior sides in the case of the ECAP-treated and double-treated workpieces, all values were within a reasonably narrow range, indicating a significant structural homogeneity enhancement after ECAP and heat treating (Fig. 14).

From the average of the hardness values, it was evident that the mean hardness of the as-received AA6061-O (60 H_v) sample improved by a factor of ~2.1 after the ECAP-treatment process (128 H_v). The heat treated samples after ECAP processing (133 H_v) revealed further improvements with regard to the mean hardness value by a factor of ~1.04 compared to the workpieces treated only by ECAP.

6. Conclusion

In this study, equal channel angular pressing (ECAP) was modified to impose severe plastic deformation on tubular AA 6061 components. The die set was designed based on results obtained via finite element analysis (FEA) with a channel angle of 120° and a corner angle of 22° that could introduce large equivalent plastic strains in a single pressing cycle, enough to refine the grains of a tubular workpiece. Hydraulic oil (SAE 30) was selected to fill the tube cavity and eliminate the possibility of tube failure as a result of buckling or fracture during the ECAP process. In addition to ECAP, a heat treatment (HT) process using the T6 method was applied to the ECAP-treated workpieces to investigate the influence of double-treatment (ECAP + heat-treating) on the mechanical properties and microstructure evolution.

A numerical simulation of the deformation mechanisms and accumulation of equivalent plastic strain (EPS) via FEA-analysis, in addition to experimental tests, including microstructure analysis, torsion, and hardness tests can be summarized as follows:

1. Plastic instability analysis demonstrated the validity of the proposed SPD process of tubes through ECAP since the triaxiality index never exceeded EPS and exhibited negative values as soon as shearing occurred.
2. The yield shear strength, ultimate shear strength, and hardness of tubular AA 6061 increased significantly for the ECAP-treated tubes by factors of ~2.5, ~1.4, and ~2.1, respectively, compared with the as-received material due to a 60% reduction in the mean grain size. However, a decrease in ductility was observed for the ECAP-treated samples compared to the as-received workpiece.
3. Heat treating (T6) performed after the ECAP process successfully recovered the ductility of the ECAP-treated workpieces. Moreover the double treatment exhibited a notably positive influence on the mechanical properties including the yield shear strength and yield ultimate strength.

Acknowledgments

This research was funded by the Ministry of Higher Education, Malaysia, with high impact research (HIR) grant numbers HIR-MOHE-16001-D000001. The work was also supported by the Human Resources Program in Energy Technology of the Korea Institute of Energy Technology Evaluation and Planning (KETEP), granted financial resource from the Ministry of Trade, Industry & Energy, Republic of Korea (No. 20154030200900).

References

- [1] R. Valiev, Y. Estrin, Z. Horita, T. Langdon, M. Zehetbauer, Y. Zhu, Fundamentals of superior properties in bulk nanoSPD materials, *Math. Res. Lett.* (2015) 1–21.
- [2] A. Azushima, R. Kopp, A. Korhonen, D.Y. Yang, F. Micari, G.D. Lahoti, et al., Severe plastic deformation (SPD) processes for metals, *CIRP Ann.* 57 (2008) 716–735.

- [3] R.Z. Valiev, Y. Estrin, Z. Horita, T.G. Langdon, M.J. Zehetbauer, Y.T. Zhu, Producing bulk ultrafine-grained materials by severe plastic deformation, *JOM* 58 (2006) 33–39.
- [4] D. Jafarlou, E. Zalnezhad, A. Hamouda, G. Faraji, N. Mardi, M.M. Hassan, Evaluation of the mechanical properties of AA 6063 processed by severe plastic deformation, *Metall. Mater. Trans. A* (2015) 1–13.
- [5] R. Valiev, Nanostructuring of metals by severe plastic deformation for advanced properties, *Nat. Mater.* 3 (2004) 511–516.
- [6] Y. Estrin, A. Vinogradov, Extreme grain refinement by severe plastic deformation: a wealth of challenging science, *Acta Mater.* 61 (2013) 782–817.
- [7] G. Faraji, M.M. Mashhadi, H.S. Kimb, Tubular channel angular pressing (TCAP) as a novel severe plastic deformation method for cylindrical tubes, *Mater. Lett.* 65 (2011) 3009–3012.
- [8] M.H. Farshidi, M. Kazeminezhad, H. Miyamoto, Microstructural evolution of aluminum 6061 alloy through tube channel pressing, *Mater. Sci. Eng. A* 615 (2014) 139–147.
- [9] L.S. Tóth, M. Arzaghi, J.J. Fundenberger, B. Beausir, O. Bouaziz, R. Arruffat-Massion, Severe plastic deformation of metals by high-pressure tube twisting, *Scr. Mater.* 60 (2009) 175–177.
- [10] A. Babaei, M.M. Mashhadi, Tubular pure copper grain refining by tube cyclic extrusion–compression (TCEC) as a severe plastic deformation technique, *Prog. Nat. Sci. Mater. Int.* 24 (2014) 623–630.
- [11] Q. Xia, G. Xiao, H. Long, X. Cheng, B. Yang, A study of manufacturing tubes with nano/ultrafine grain structure by stagger spinning, *Mater. Des.* 59 (2014) 516–523.
- [12] V.M. Segal, Equal channel angular extrusion: from macromechanics to structure formation, *Mater. Sci. Eng. A* 271 (1999) 322–333.
- [13] A.V. Nagasekhar, U. Chakkingal, P. Venugopal, Candidature of equal channel angular pressing for processing of tubular commercial purity-titanium, *J. Mater. Process. Technol.* 173 (2006) 53–60.
- [14] F. Djavanroodi, A. Zolfaghari, M. Ebrahimi, K. Nikbin, Equal channel angular pressing of tubular samples, *Acta Metall. Sin.* 26 (2013) 574–580 (English Letters).
- [15] W.S. Miller, L. Zhuang, J. Bottema, A.J. Wittebrood, P.D. Smet, A. Haszler, et al., Recent development in aluminium alloys for the automotive industry, *Mater. Sci. Eng. A* 280 (2000) 37–49.
- [16] A. Heinz, A. Haszler, C. Keidel, S. Moldenhauer, R. Benedictus, W.S. Miller, Recent development in aluminium alloys for aerospace applications, *Mater. Sci. Eng. A* 280 (2000) 102–107.
- [17] F. Ozturk, A. Sisman, S. Toros, S. Kilic, R.C. Picu, Influence of aging treatment on mechanical properties of 6061 aluminum alloy, *Mater. Des.* 31 (2010) 972–975.
- [18] E8/E8M-11. Standard test methods for tensile testing of metallic materials. ASTM International, West Conshohocken, PA. 2011, www.astm.org.
- [19] Q.X. Pei, B.H. Hu, C. Lu, Y.Y. Wang, A finite element study of the temperature rise during equal channel angular pressing, *Scr. Mater.* 49 (2003) 303–308.
- [20] E143-13. Standard test method for shear modulus at room temperature. ASTM International, West Conshohocken, PA. 2013, www.astm.org.
- [21] G.E. Dieter, D. Bacon, *Mechanical Metallurgy*, McGraw-Hill, New York, 1986.
- [22] A. Babaei, M.M. Mashhadi, H. Jafarzadeh, Tube cyclic expansion–extrusion (TCEE) as a novel severe plastic deformation method for cylindrical tubes, *J. Mater. Sci.* 49 (2014) 3158–3165.
- [23] S. Arsene, J. Bai, A new approach to measuring transverse properties of structural tubing by a ring test: experimental investigation, *J. Test. Eval.* 26 (1998) 26–30.
- [24] E384-11e1. Standard Test Method for Knoop and Vickers Hardness of Materials. ASTM International, West Conshohocken, PA. 2011, www.astm.org.
- [25] D. Jafarlou, E. Zalnezhad, M. Ezazi, N. Mardi, M. Hassan, The application of equal channel angular pressing to join dissimilar metals, aluminium alloy and steel, using an Ag–Cu–Sn interlayer, *Mater. Des.* 87 (2015) 553–566.
- [26] G.E. Totten, S.E. Westbrook, R.J. Shah, *Fuels and Lubricants Handbook – Technology, Properties, Performance, and Testing* (MNL 37WCD), ASTM International, 2003.
- [27] Y. Iwahashi, J. Wang, Z. Horita, M. Nemoto, T.G. Langdon, Principle of equal-channel angular pressing for the processing of ultra-fine grained materials, *Scr. Mater.* 35 (1996) 143–146.
- [28] M.S. Mohebbi, A. Akbarzadeh, Accumulative spin-bonding (ASB) as a novel SPD process for fabrication of nanostructured tubes, *Mat. Sci. Eng. A Struct.* 528 (2010) 180–188.
- [29] C. Xu, Z. Horita, T.G. Langdon, The evolution of homogeneity in processing by high-pressure torsion, *Acta Mater.* 55 (2007) 203–212.
- [30] S. Li, M.A.M. Bourke, I.J. Beyerlein, D.J. Alexander, B. Clausen, Finite element analysis of the plastic deformation zone and working load in equal channel angular extrusion, *Mater. Sci. Eng. A* 382 (2004) 217–236.
- [31] R.H. Wagoner, J.-L. Chenot, *Fundamentals of Metal Forming*, John Wiley & Sons Inc., New York, 1996.
- [32] Y. Bao, T. Wierzbicki, On fracture locus in the equivalent strain and stress triaxiality space, *Int. J. Mech. Sci.* 46 (2004) 81–98.
- [33] J.W. Hancock, A.C. Mackenzie, On the mechanisms of ductile failure in high-strength steels subjected to multi-axial stress-states, *J. Mech. Phys. Solids* 24 (1976) 147–160.
- [34] H. Pouraliakbar, S. Firooz, M.R. Jandaghi, G. Khalaj, A. Amirafshar, Combined effect of heat treatment and rolling on pre-strained and SPDed aluminum sheet, *Mater. Sci. Eng. A* 612 (2014) 371–379.
- [35] V.L. Tellkamp, E.J. Lavermia, A. Melmed, Mechanical behavior and microstructure of a thermally stable bulk nanostructured Al alloy, *Metall. Mater. Trans. A* 32 (2001) 2335–2343.
- [36] Y. Wang, M. Chen, F. Zhou, E. Ma, High tensile ductility in a nanostructured metal, *Nature* 419 (2002) 912–915.
- [37] D.J. Dunstan, A.J. Bushby, Grain size dependence of the strength of metals: the Hall–Petch effect does not scale as the inverse square root of grain size, *Int. J. Plast.* 53 (2014) 56–65.

- [38] R.Z. Valiev, I.V. Alexandrov, Y.T. Zhu, T.C. Lowe, Paradox of strength and ductility in metals processed by severe plastic deformation, *J. Mater. Res.* 17 (2002) 5–8.
- [39] Y. Estrin, A. Vinogradov, Fatigue behaviour of light alloys with ultrafine grain structure produced by severe plastic deformation: an overview, *Int. J. Fatigue* 32 (2010) 898–907.
- [40] H. Schmidt, Winterstetter TA, Spon press, *Buckling of Thin Metal Shells*, 2004.
- [41] T.A. Winterstetter, H. Schmidt, Beulversuche an längsnahtgeschweißten stählernen KZS im elastisch-plastischen Bereich unter Axialdruck, Innendruck und Torsionsschub, Dept. of Civil Eng., University of Essen, 1999 82.
- [42] T.R. Malow, C.C. Koch, Mechanical properties, ductility, and grain size of nanocrystalline iron produced by mechanical attrition, *Metall. Mater. Trans. A* 29 (1998) 2285–2295.